Spectral crossovers and universality in quantum spin chains coupled to random fields

Debojyoti Kundu [*], Santosh Kumar [†], and Subhra Sen Gupta [‡]

Department of Physics, Shiv Nadar University, Gautam Buddha Nagar, Uttar Pradesh 201314, India

We study the spectral properties of and spectral crossovers between different random matrix ensembles [Poissonian, Gaussian orthogonal ensemble (GOE), Gaussian unitary ensemble (GUE)] in correlated spin-chain systems, in the presence of random magnetic fields, and the scalar spin-chirality term, competing with the usual isotropic and time-reversal invariant Heisenberg term. We have investigated these crossovers in the context of the *level-spacing distribution* and the *level-spacing ratio distribution*. We use random matrix theory (RMT) analytical results to fit the observed Poissonian-to-GOE and GOE-to-GUE crossovers, and examine the relationship between the RMT crossover parameter λ and scaled physical parameters of the spin-chain systems in terms of a scaling exponent. We find that the crossover behavior exhibits *universality*, in the sense that, it becomes independent of lattice size in the large Hamiltonian matrix dimension limit. Moreover, the scaling exponent obtained from such a finite size scaling analysis, seems to be quite robust and independent of the type of crossover considered or the specific spectral correlation measure used.

I. INTRODUCTION

The Hubbard model and some of its generalizations [1–4] are prototypical models for interacting electrons moving in a highly correlated manner, on a lattice. It is well known that under certain conditions like large local (onsite) Coulomb repulsion and for an integer number of electrons per lattice site, the *charge* degrees of freedom are frozen out (no net number and hence charge fluctuations at sites, to a first approximation) while the *spin* and the *orbital* degrees of freedom remain active via relative change in intrasite spin-orbital occupancies. This results in effective spin-orbital intersite exchange interactions leading to Anderson superexchange [5–7] and Kugel-Khomskii–like [8,9] physics. For the single-band Hubbard model, or for multiband models with very large Hund's coupling, orbital fluctuations are irrelevant and this leads to a variety of spin-only Hamiltonians, the most basic of which is the *isotropic Heisenberg model*. While the parent fermionic models are difficult or impossible to solve exactly, especially in higher dimensions, even the effective spin Hamiltonians embody very rich physics and often do not yield to exact solutions, especially in the presence of spin-orbit coupling and magnetic-field-induced anisotropies [10–16]. Numerical solutions become very important in these circumstances.

Another central paradigm of modern condensed matter physics is the presence of disorder. While the problem of disorder (random site and bond energies mimicking impurities in real solids) in absence of interactions was addressed a long time ago by Anderson and coworkers [17–20], the generic problem of disorder in the presence of electron correlations is a very difficult one and only limited success has been achieved [21–24]. In this regime one has to depend even more on numerical methods, which are further complicated by an exponentially growing basis size and the need to perform some kind of averaging over numerous disordered configurations.

One of the techniques that can be used to study the physics of such systems is random matrix theory (RMT) [25–29], which deals with the statistical properties of eigenvalues and eigenfunctions of matrices, with random-valued elements. Since the Hamiltonians for disordered, interacting systems involve very large matrices with random entries, the connection becomes apparent. In recent times there have been several studies in this direction [30–36]. In this paper we investigate the systematics of eigenvalue statistics in Heisenberg spin chains, in the presence of a random inhomogeneous magnetic field, and the scalar-chirality three-spin interaction, whose various limits lead to the preservation or breaking of various unitary and antiunitary symmetries, leading to various eigenvalue statistics which can be described by random matrix ensembles with appropriate symmetry properties, as detailed below [25–28,37].

Wigner first introduced RMT in physics in the context of explaining the statistical properties of nuclear spectra [38–40]. Since then RMT has been successfully applied in the spectral study of various disordered systems, quantum chaotic systems, and large complex atoms and molecules [25,27,41]. It has also found its application in stock-market data analysis, atmospheric science, medical science, and in many more fields [29,42–44]. The valuable contributions of Wigner and Dyson in explaining complex energy levels of large nuclei [45–49], provide deep insights into the generic properties of energy spectra of physical many-body quantum systems. Dyson pioneered the classification of random matrix ensembles via his

---

[*]debojyoti.kundu.physics@gmail.com

[†]Corresponding author: skumar.physics@gmail.com

[‡]Corresponding author: subhro.sengupta@gmail.com

famous *threefold way* [37,49], depending on the presence or absence of various unitary (mainly rotations) and antiunitary (time-reversal) symmetries in the system. The representation of most physical Hamiltonians, rendered nonintegrable due to the presence of random components like disorder, involve relatively large matrices with random entries, and hence the spectral properties of such systems fall well within the ambit of RMT. Spacing distribution of energy levels in RMT plays a decisive role as an indicator of integrability of a quantum many-body system [50–54]. The Berry-Tabor conjecture [55] and the BGS (Bohigas, Giannoni, and Schmit) conjecture [56] asserted that the distribution of level spacings of an integrable and a nonintegrable quantum system follow the Poissonian and the Wigner-Dyson distributions, respectively. Generally, there is no single definition of integrability [57] of a quantum system (or the fact as to whether the system is exactly solvable or not): one popular practice is to represent this in terms of thermalization [54]. Classically, thermalization of a system is dictated by its dynamical chaotic behavior, ergodicity, etc [58–60]. Classical chaotic systems are nonintegrable in nature. But there is no such obvious feature which leads to the thermalization in quantum many-body systems [61,62]. Quantum integrable systems are comprised of a large number of physical operators (conserved quantities) in the thermodynamic limit [63,64], that commute with the system Hamiltonian. On the other hand, quantum nonintegrable systems do not have an extensive number of conserved quantities and their dynamics is not strictly guided by conservation laws [61,65,66].

In RMT, nearest-neighbor spacing distribution (NNSD), viz., the distribution of spacings between consecutive eigenvalues, is commonly used to study the local fluctuations in the eigenspectrum. Depending upon the underlying symmetries, and the correlations among the eigenvalues, universal features associated with Poissonian statistics, Gaussian orthogonal ensemble (GOE) statistics, Gaussian unitary ensemble (GUE) statistics, or Gaussian symplectic ensemble (GSE) statistics, can follow. When the eigenvalues are uncorrelated, the NNSD follows the Poissonian distribution. Whereas NNSD of correlated eigenvalues follows one of the three above-mentioned Gaussian statistics [25,49,67]. In real physical systems, the preservation or breaking of various unitary and antiunitary symmetries (like time-reversal symmetry, unconventional time-reversal symmetry, rotational symmetry, etc.), leads the spectral fluctuations to follow one of the above-mentioned statistics. For example, the NNSD computed using the spectra of heavy nuclei [45–49], chaotic billiards [68,69], nonintegrable spin chains [30,31,33], Sachdev-Ye-Kitaev (SYK) Hamiltonian [70], etc., all agree with the *Wigner-surmise* results for NNSD [25–27]. In addition, there can be circumstances when there is a "*partial breaking*" of a symmetry which results in the system spectra to follow an *intermediate statistics* [25,27,31,33,71–75]. These systems are analyzed via crossover random matrix models or RMT interpolating functions [28,31,72,75–83] that depend on symmetry-breaking or RMT crossover parameters (discussed in Sec. III A). Limiting values of these parameters lead to the two extremes of the concerned symmetry crossover. These RMT crossover parameters can often be associated with certain physical parameters of the system under study, for instance, magnetic field, that breaks *rotational* and *time-reversal* symmetries [80,84].

The well-known *Wigner-surmise* results for NNSD (discussed in Sec. III A) can be derived using 2×2 Gaussian random matrices and serve as very good approximations to the large-dimension exact results [25,40,41,85]. Over the years, among other things, these results have been used to analyze statistical behavior of spectra from large many-body quantum systems [25,27,32]. Similar results, comprising interpolating functions, have also been empirically proposed or derived using small-dimension matrices for studying symmetry crossovers [72,81,86–88]. These Wigner-surmise-like results have been quite fruitful in examining NNSD crossovers in quantum many-body systems with stochastic interactions or couplings to random external fields. In quantifying the spectral fluctuations in symmetry crossovers, the physical symmetry-breaking parameters need to be suitably scaled, which results in the universal validity of the Wigner-surmise-like formulas, and thereby their applicability to a large variety of systems and problems ensues [72,76–79,82,89]. Some examples in this context include heavy nuclei [90], metallic ring in a magnetic field [91], metal-insulator transition [92], magnetoconductance of ballistic quantum dots [93], quantum kicked rotor [75], bipartite entanglement entropy [94], etc. NNSD crossovers can also be utilized for studying symmetry-dictated spectral crossovers in quantum spin systems [31].

In this work, we study the crossover between different random matrix ensembles using linear spin-chain models similar to the ones discussed in Refs. [30,31]. Most earlier studies, in this context, have typically used empirical or phenomenological crossover formulas. We, on the other hand, use interpolating functions based on crossover RMT models, such as the ones derived in Refs. [72,87], where the physical meaning of the symmetry-crossover parameters is lucid. We successfully map the crossovers in the physical spin-chain models onto the RMT crossover ensembles and thus corroborate the associated universality. By comparing the RMT crossover parameters with the symmetry-breaking physical parameters in spin-chain models, we identify universal scaling exponents for different NNSD crossovers in the large system size limit. In addition to NNSD, we also examine the distribution of the ratio of two consecutive level spacings. This quantity has the advantage that, unlike the computation of NNSD, it does not require the unfolding of the spectra due to the presence of nonuniform density of states (DOS). Due to this, the study of spacings-ratio related statistics has gained a lot of attention in recent years among researchers after being introduced by Oganesyan and Huse in studying statistical behavior of one-dimensional spinless-fermion model [95]. Wigner-surmise-like results for the ratio distribution (RD), based on 3×3 matrix models, are available for the three standard symmetry classes of RMT, as well as for certain crossover ensembles [75,82,96,97]. Over the years these results of ratio distribution have been successfully applied in studying statistical behavior of large quantum many-body systems like spin-chain systems [33,34,73,98–100], many-body quasiperiodic systems [35], Bose-Hubbard model [36,52], etc. Similar to NNSD, our detailed analysis of ratio distribution in spin-chain models for various symmetry crossovers and

comparison with RMT results again leads to identification of universal scaling exponents.

The presentation scheme in the rest of this paper is as follows. In Sec. II, we describe the spin-chain Hamiltonian used in our study and its various limits which give rise to distinct symmetry classes. In Sec. III we summarize the various RMT key concepts and results used in our analysis. We present our calculations and results in Sec. IV which includes, *inter alia*, a detailed explanation of the universality aspects. We conclude in Sec. V with summary and discussion of our work.

II. METHODOLOGY: THE SPIN HAMILTONIAN, ITS SYMMETRIES, THE BASIS AND CONFIGURATION AVERAGING

We consider a one-dimensional spin-$\frac{1}{2}$ Hamiltonian H, with one spin per lattice site. It consists of the usual isotropic Heisenberg term (H_h), a random term (H_r) representing the coupling of the spin system to a spatially inhomogeneous (on the length scale of lattice spacings) and random magnetic field,[1] and the three-site scalar spin-chirality term (H_c) [30,31] which appears in the third order of the strong coupling expansion of the Hubbard model for a complex hopping amplitude, induced in the presence of a magnetic field [16]. For example, this kind of spin correlation term can emerge while probing Mott insulators using circularly polarized laser [101]. We have

$$H = H_h + H_r + H_c$$
$$= \sum_{j=1}^{N-1} J\mathbf{S}_j \cdot \mathbf{S}_{j+1} + \sum_{j=1}^{N} h_j S^z{}_j + \sum_{j=1}^{N-2} J_t \mathbf{S}_j \cdot [\mathbf{S}_{j+1} \times \mathbf{S}_{j+2}].$$
$$(1)$$

This Heisenberg spin-$\frac{1}{2}$ chain consists of N sites, $\mathbf{S}_j$ is the spin operator at site j, and J is the nearest-neighbor exchange interaction. A Zeeman-like coupling of the spin chain to an external stochastic magnetic field, is introduced via the random term H_r, where h_j is the random magnetic field along the z direction at site j, which follows a Gaussian distribution having zero mean and variance h^2 [30]. The three-site interacting scalar spin-chirality term [13–16] H_c is also included in our Hamiltonian, with a coupling constant J_t. This term can

be simplified as[2]

$$J_t \mathbf{S}_j \cdot [\mathbf{S}_{j+1} \times \mathbf{S}_{j+2}] = \frac{1}{2} \sum_{k,l,m} iJ_t \varepsilon_{klm} S^z_k S^+_l S^-_m, \quad (2)$$

where ε_{klm} is the standard Levi-Civita symbol and each of k, l, and m takes the values j, $j + 1$ and $j + 2$ (see the Appendix for a derivation). This term favors a noncoplanar arrangement of spins and hence counters the other two terms in this sense. All other interactions in the Hamiltonian are expressed in units of the Heisenberg coupling J throughout this paper (so effectively $J = 1.0$).

It is well known from the literature [25,26,49,67] that the eigenvalues of an integrable system are uncorrelated, therefore, the eigenvalue-spacing distribution of the Hamiltonian is Poissonian. For the nonintegrable systems, on the other hand, the presence or absence of various unitary and antiunitary symmetries drive the eigenvalue spacings of the system Hamiltonian to follow different Gaussian ensemble distributions, as described below.

Any angular momentum operator $\mathcal{J}$ is odd under the usual time-reversal symmetry operation, i.e., $T_0 \mathcal{J} T_0^{-1} = -\mathcal{J}$. The *antiunitary* time-reversal operator for a spin-$\frac{1}{2}$ system is defined as $T_0 = e^{i\pi S^y/\hbar} K$ where S^y is the y component of spin operator and K is the *complex-conjugation* operator. The spin, being an angular momentum, is odd under time reversal and for a particular term of a spin Hamiltonian, the *evenness* or *oddness* under the time-reversal symmetry depends on the number of the spin operators involved in that term. H_h is time-reversal-symmetry invariant (or even) ($T_0 H_h T_0^{-1} = H_h$), as it involves *two* spin operators. But, H_r and H_c are odd under time reversal as the number of the spin operators involved in these terms is odd (*one* and *three*, respectively). The *unconventional time-reversal symmetry* is discussed in Refs. [26,30,31], where the antiunitary unconventional time-reversal operator is defined by $T = e^{i\pi S^x/\hbar} T_0$. H_h and H_r are even and H_c is odd under the unconventional time-reversal symmetry. This is because the unitary operator $e^{i\pi S^x/\hbar}$ reverses the signs of S^y_j and S^z_j but not of S^x_j. So, in totality, T reverses the sign of S^x_j alone. Thus, the full Hamiltonian H is neither even nor odd under these antiunitary symmetry operations.

Now, when only the Heisenberg term is present in Eq. (1), the Hamiltonian of the system is preserved under both antiunitary symmetries T_0 and T. So the eigenvalues of the Hamiltonian matrix are uncorrelated and the level spacings are expected to follow the Poissonian distribution. If we switch on H_r, then T_0 is broken but the Hamiltonian $H_1 (= H_h + H_r)$ is still invariant under T. The Hamiltonian matrix becomes real symmetric and the correlation statistics of the eigenvalues should follow the GOE distribution. When all the three terms of Eq. (1) are present, both antiunitary symmetries are broken and the matrix representation of H becomes complex Hermitian [complex nature is introduced by the scalar-chirality term, apparent from Eq. (2)]. The correlation statistics of the eigenvalues should now follow GUE distribution. By varying the relative amplitudes of each term in H, we can achieve

---

[1]This microscale inhomogeneity is essential to observe the spectral crossovers that we intend to study because if one uses a random but spatially uniform (again on the length scale of the lattices that we use), the Zeeman term simplifies to the product of the uniform field amplitude (h_z) times the total S^z of the lattice. Such a term has no effect at all when we restrict ourselves to the $S^z = 0$ sector of a lattice with an *even number of sites* and the system will always remain in the Poissonian regime. Even for a lattice with an *odd number of sites*, for which the lowest sector is $S^z = \frac{1}{2}$, such a field amounts to a uniform shift of *all* energy levels, that does not alter the level spacings or their ratios (as these are calculated within a given realization of the random field), in which we are interested. So again no crossovers from the Poissonian regime will be observed.

[2]The $\frac{1}{2}$ factor in the simplified form is missing in Refs. [30,31]. See the Appendix for derivation.

crossovers between the Poissonian, GOE, and GUE distributions.

To construct the basis for our exact diagonalization calculations, we consider a spin-chain system with a spin $\frac{1}{2}$ at each lattice site. That means each of the N sites of the system can be occupied by either of an up spin ($m^z = \frac{1}{2} \equiv \uparrow$) or a down spin ($m^z = -\frac{1}{2} \equiv \downarrow$), where m^z is the eigenvalue of S^z. There exist 2^N number of basis states ($|m_1^z m_2^z m_3^z \ldots m_N^z\rangle$) for an N-site system. Here we can see that $[S^2, H] \neq 0$ (where S^2 is the square of the total spin operator with $\mathbf{S} = \sum_{j=1}^N \mathbf{S}_j$) but $[S^z, H] = 0$ (where the total z component of spin $S^z = \sum_{j=1}^N S_j^z$). So among the total 2^N number of basis states we only consider a subspace having a constant S^z value. In our calculations we have considered systems where N is *even* and we restrict ourselves to the $S^z = 0$ subspace, which includes contributions from all total S sectors and has the largest dimension ($n = C_{N/2}^N$). As we are considering the whole spectrum, the sign of J is irrelevant unlike in ground-state studies. We have used full exact diagonalization methods to obtain the energy eigenvalues and eigenfunctions, as we need the full spectrum of eigenvalues. This consequently limits the system sizes that we can access, to some extent, but manages to capture the universality behavior that we demonstrate in this work.

Since we are considering the system in the presence of a random, inhomogeneous magnetic field, one typically needs to average over several random configurations or realizations of the magnetic field, in order to obtain good spectral statistics. In a real-life experimental situation, this could be due to the coupling of the system to an external magnetic field, fluctuating rapidly on the timescale of a typical magnetic measurement. This means that any measured physical quantity is essentially time averaged over several configurations of this rapidly fluctuating magnetic field, which is mimicked by an ensemble average over several random configurations in our calculations, implicitly implying usual statistical *ergodicity* [58–60]. Each *configuration*, for a given h (standard deviation of the Gaussian distribution from which the magnetic fields are drawn), consists of a set of N site magnetic fields $\{h_j\}$. For each such set, the Hamiltonian is diagonalized in the above basis and the energy spacings are computed and stored. For the purposes of configuration averaging, we consider a set of $\mathcal{M}$ such configurations, henceforth referred to as an *ensemble*. This diagonalization and computation of spacings is repeated for each member of the ensemble, and the final set of all energy spacings from all the configurations is used to plot the histogram (distribution) of energy spacings. As h is varied over some suitable grid, the entire process above is repeated and a level-spacing distribution is obtained for each h. Details of the exact number of configurations used in an ensemble, for each lattice size, are discussed in Sec. IV. We find that the larger the lattice size (and hence the basis size), the smaller the number of configurations are needed to obtain good statistics or, equivalently, a smooth distribution profile. This indeed reflects the "self-averaging" or the "spectral ergodicity" property of RMT, which demonstrates the equivalence of the ensemble average and the spectral average, in the limit of large Hamiltonian matrices [26,102]. This also applies to the spectral studies of disordered many-body quantum systems for subspaces with relatively large basis sizes [103,104].

TABLE I. Probability distribution of nearest-neighbor spacings for unfolded eigenvalues [25,26].

Type of distribution	NNSD probability density
Poissonian	$P_{\text{Poi}}(s) = \exp(-s)$
GOE	$P_{\text{GOE}}(s) = (\pi s/2) \exp(-\pi s^2/4)$
GUE	$P_{\text{GUE}}(s) = (32 s^2/\pi^2) \exp(-4 s^2/\pi)$

III. RANDOM MATRIX THEORY (RMT)

In this section, we summarize the RMT results which are required for the analysis of our results. These include the exact expressions for the nearest-neighbor spacing distributions and ratio distributions, for invariant as well as crossover ensembles.

A. Nearest-neighbor spacing distribution (NNSD)

In RMT, the fluctuation properties of a system's eigenspectrum are quantified using both short-range and the long-range level statistics [25,26]. NNSD is the most widely studied statistical measure to quantify the local correlations among energy eigenvalues of a given system. Since the DOS is nonuniform for the eigenspectrum of an arbitrary physical system, one requires to implement the unfolding procedure to compare the calculated fluctuations with the standard RMT results. In our analysis pertaining to NNSD, we use polynomial fits to the calculated DOS and use it to unfold the spectra [25,26,30,80]. If the ordered sequence of n energy eigenvalues of a Hamiltonian is given by $\varepsilon_1 < \cdots < \varepsilon_n$, then the unfolded eigenvalues are calculated using $\tilde{\varepsilon}_j = n \int_{\varepsilon_1}^{\varepsilon_j} \rho(\varepsilon) d\varepsilon$, where $\rho(\varepsilon) = d\mathcal{N}(\varepsilon)/d\varepsilon$ is the fitted DOS, and $\mathcal{N}(\varepsilon)$ is the cumulative DOS. The nearest-neighbor level spacing of the unfolded eigenvalues is defined as $s_j = \tilde{\varepsilon}_{j+1} - \tilde{\varepsilon}_j$. The corresponding frequency distribution, or rather its fitted envelope [$P(s)$], is then compared with the RMT analytical results for its quantification, as discussed in the Introduction. The Wigner surmise expressions for the three Dyson symmetry classes along with the Poisson distribution are compiled in Table I, for this purpose.

In this paper, we are interested in studying crossover between different RMT ensembles. It is modeled using the Pandey-Mehta Hamiltonian [78,79,105]

$$\mathcal{H} = \frac{\mathcal{H}_0 + \lambda \mathcal{H}_\infty}{\sqrt{1 + \lambda^2}}, \qquad (3)$$

wherein the symmetry of the primary Hamiltonian $\mathcal{H}_0$ is broken by the perturbing Hamiltonian $\mathcal{H}_\infty$, with the extent of this symmetry breaking being controlled by the crossover parameter λ. The two extremes of $\mathcal{H}$, viz., $\mathcal{H}_0$ and $\mathcal{H}_\infty$, belonging to two different symmetry classes, are obtained for $\lambda = 0$ and $\lambda \to \infty$. Our focus in the current work is on examining the Poissonian-to-GOE and GOE-to-GUE crossovers, which is achieved by tuning the crossover parameter. The Wigner-surmise-like results for the spacing distributions have been derived in Ref. [72] for these crossovers. The NNSD function interpolating between the Poissonian and the GOE

TABLE II. Probability distribution of ratio of consecutive spacings [96,97].

Type of distribution	RD probability density
Poissonian	$\mathcal{P}_{\text{Poi}}(r) = 1/(1+r)^2$
GOE	$\mathcal{P}_{\text{GOE}}(r) = 27r(r+1)/[8(r^2+r+1)^{5/2}]$
GUE	$\mathcal{P}_{\text{GUE}}(r) = 81\sqrt{3}r^2(r+1)^2/[4\pi(r^2+r+1)^4]$

distributions is given by [72,106]

$$f_{P\to O}(\lambda, s) = \frac{su^2(\lambda)}{\lambda}\exp\left(-\frac{u^2(\lambda)s^2}{4\lambda^2}\right)$$
$$\times \int_0^\infty \exp(-x^2 - 2x\lambda)I_0\left(\frac{sxu(\lambda)}{\lambda}\right)dx. \quad (4)$$

Here, $I_0(z)$ is the modified Bessel function and $u(\lambda) = \sqrt{\pi}U(-\frac{1}{2}, 0, \lambda^2)$, with $U(a, b, z)$ being the confluent hypergeometric function of the second kind (Tricomi function). The limiting cases of $\lambda \to 0$ and $\lambda \to \infty$ lead to the Poissonian and the GOE spacing distributions, respectively, as shown in Table I. Similarly, the interpolating function for GOE-to-GUE crossover is given by [72,106]

$$f_{O\to U}(\lambda, s) = \left(\frac{2+\lambda^2}{2}\right)^{1/2} D^2(\lambda)$$
$$\times s\exp\left(\frac{s^2 D^2(\lambda)}{2}\right)\text{erf}\left(\frac{sD(\lambda)}{\lambda}\right), \quad (5)$$

where

$$D(\lambda) = \left(\frac{\pi(2+\lambda^2)}{4}\right)^{1/2}\left[1 - \frac{2}{\pi}\left\{\arctan\left(\frac{\lambda}{\sqrt{2}}\right) - \frac{\sqrt{2}\lambda}{2+\lambda^2}\right\}\right].$$

In this case, the limits $\lambda \to 0$ and $\lambda \to \infty$ result in the GOE and the GUE spacing distributions, respectively, as given in Table I. These interpolating functions are based on 2×2 matrix models, however, once the transition parameter is suitably scaled, these results can be applied to larger dimensional cases also [80,81,106–113]. One of our key objectives in this paper is to probe such a scaling for spin-chain systems.

B. Ratio distribution (RD)

As discussed in the Introduction, another short-range fluctuation measure which circumvents the need of unfolding and has become quite popular in recent times is the distribution of the ratios of consecutive level spacings [33,34,73,95–97,114]. Considering again the ordered sequence of n energy eigenvalues $\varepsilon_1 < \cdots < \varepsilon_n$, one examines the distribution of the ratio of two consecutive level spacings given by $r_j = (\varepsilon_{j+2} - \varepsilon_{j+1})/(\varepsilon_{j+1} - \varepsilon_j)$. The RMT results for the ratio distribution $\mathcal{P}(r)$, based on 3×3 matrix models, have been derived for the three standard symmetry classes, along with the Poissonian case in Ref. [96]. These are analogous to the results for NNSD and are compiled in Table II. A related quantity is $\tilde{r} = \min(r, 1/r)$, which is also used quite often as this quantity gets restricted in the interval [0,1], and the corresponding probability distribution is $\tilde{\mathcal{P}}(\tilde{r}) = 2\mathcal{P}(\tilde{r})\Theta(1 - \tilde{r})$.

As far as the crossover is concerned, there are several phenomenological formulas available for the RD (see, for

example, Refs. [33,73,114]). However, we are interested in results based on RMT crossover model as in Eq. (3). In this context, to the best of our knowledge, there is no result available for the Poissonian-to-GOE crossover and we resort to numerics. On the other hand, an exact expression for the ratio distribution, based on a 3×3 matrix model, is known for the GOE-to-GUE crossover [75]. It is given by the following interpolating function:

$$\mathcal{F}_{O\to U}(\lambda, r) = \frac{r(1+r)}{16\sqrt{6\pi}}(1+\lambda^2)^{3/2}$$
$$\times [g(a, b) + g(a, br) - g(a, br + b)], \quad (6)$$

where

$$g(\eta, \xi) = \frac{\xi(5\eta^2 + 3\xi^2)}{\eta^4(\eta^2 + \xi^2)^2} + \frac{3}{\eta^5}\arctan\left(\frac{\xi}{\eta}\right),$$

$a(r) = \sqrt{(1 + r + r^2)/6}$ and $b(\lambda) = 1/(2\sqrt{2}\lambda)$. When $\lambda \to 0$ this interpolating function follows GOE statistics and for $\lambda \to \infty$ it follows GUE statistics, as given in Table II. Similar to the case of NNSD, when applied to large-dimensional matrices, the crossover parameter λ in the above expressions needs to be scaled properly as we will see in Sec. IV B.

IV. CALCULATIONS AND RESULTS

In this section, we present the details of our calculations and various results concerning RMT analysis of the spin-chain system for the various symmetry crossovers.

A. Nearest-neighbor spacing distribution (NNSD)

We consider nearest-neighbor spacings of energy eigenvalues computed from the Hamiltonian matrix H by its numerical diagonalization and analyze its statistics. We notice that level-spacing distributions for spin-chain systems with lattice size $N = 14$ (matrix dimension for the $S^z = 0$ subspace, $n = 3432$) and above, follow standard RMT results.[3] So, we carry out calculations for spin chains having $N = 14$ and 16 ($n = 12\,870$) sites, on an ensemble of $\mathcal{M} = 50$ and 10 matrices, respectively. Also, performing diagonalization for systems having $N = 18$ ($n = 48\,620$) or more, is computationally very expensive, so we do not attempt the full basis calculation, but resort to a reduced basis calculation, based on spin-inversion symmetry consideration, as discussed later. Periodic boundary conditions give rise to extra degeneracies in the spectra and, therefore, we consider open boundary condition throughout our calculations. We have unfolded the system spectra using polynomial fits (as mentioned in Sec. III A) to obtain unfolded spectra for which the average spacing equals unity.

1. Poissonian-to-GOE crossover

To realize Poissonian-to-GOE crossover we proceed as follows. To begin with, we switch off the scalar chirality term ($J_t = 0$) and the random field term ($h = 0$). In this setting,

---

[3]We have studied the level-spacing statistics for smaller systems having $N = 10$ ($n = 252$) and $N = 12$ ($n = 924$); they do not follow the standard RMT ensembles, closely enough.

the system is integrable and NNSD obeys Poissonian level-spacing distribution [$P_{Poi}(s)$], as expected. We then switch on the random term and vary the magnetic field values h_j on the sites. As mentioned earlier, these are drawn from the Gaussian distribution with mean zero and standard deviation h. This introduces disorder in the system and the system becomes nonintegrable. Each set $\{h_j\}$ of the N random site fields corresponds to one member of the aforesaid ensemble or one realization of disorder, as already discussed earlier. As the magnitude of h is gradually increased, a crossover from Poissonian to GOE statistics is observed. After a certain value of h, the regime beyond the applicability of RMT is reached and the statistics reverts back to Poissonian, due to *localization of eigenstates*. This simply means that, due to a very high magnetic field, the quantum fluctuation effects included in the Heisenberg term are strongly suppressed, and consequently the weights of the eigenstates spread over a much fewer number of basis configurations now. In Fig. 1 we show this Poissonian→GOE→Poissonian (integrable→quantum chaotic→integrable) transition with the increasing random magnetic field value.

To estimate the threshold for the magnetic field at which the Poisson-GOE crossover is more or less complete, we evaluate the Kullback-Leibler divergence (KL divergence) [115–117] of the calculated spacing distribution $P(s)$ at different values of h, with respect to $P_{GOE}(s)$. This comparison is shown in Fig. 2 for the $N = 14$ and 16 systems. The KL divergence is a measure of the difference between two probability distributions. Let us say p and q are the two probability distributions in question, then the KL divergence of q relative to p is given by

$$D_{KL}(p||q) = \int dx\, p(x) \ln\left(\frac{p(x)}{q(x)}\right). \tag{7}$$

For our computation, we use the discretized version of this formula. When the two distributions are same, i.e., $p = q$, the KL divergence is *zero*, and for very distinct distributions, it assumes a high value. Here, the two extreme cases correspond to Poissonian and GOE distributions for which KL divergence has a value ~ 0.28 [using the analytical forms $P_{Poi}(s)$ and $P_{GOE}(s)$, from Table I]. In Fig. 2, we observe that these extreme KL divergence values are 0.24 and 0.26 for the $N = 14$ and 16 systems, respectively, converging towards the aforesaid theoretical value of ~ 0.28.

From Fig. 2 we estimate that the Poissonian-to-GOE crossover is achieved at about $h = 0.17$ and 0.13 for the $N = 14$ and 16 systems, respectively. Beyond the crossover value of h, the systems enter in the GOE regime and KL divergence saturates near zero as observed in Fig. 2.

Next, we plot the NNSD for the Poissonian-to-GOE crossover for $N = 14$ (Fig. 3) and $N = 16$ (Fig. 4) systems, and find out that both systems reach GOE at external magnetic field values which are estimated from the KL divergence calculation as $h \sim 0.17$ and $h \sim 0.13$, respectively. We observe here that *with increasing system size we need a lesser magnitude of the symmetry-breaking random magnetic field*, which is in agreement with RMT crossover studies in Refs. [77,78,89]. We now fit the RMT interpolating function $f_{P\to O}(\lambda, s)$ of Eq. (4) to these computed distributions to obtain the values of the RMT crossover parameter λ, vis-a-vis the physical
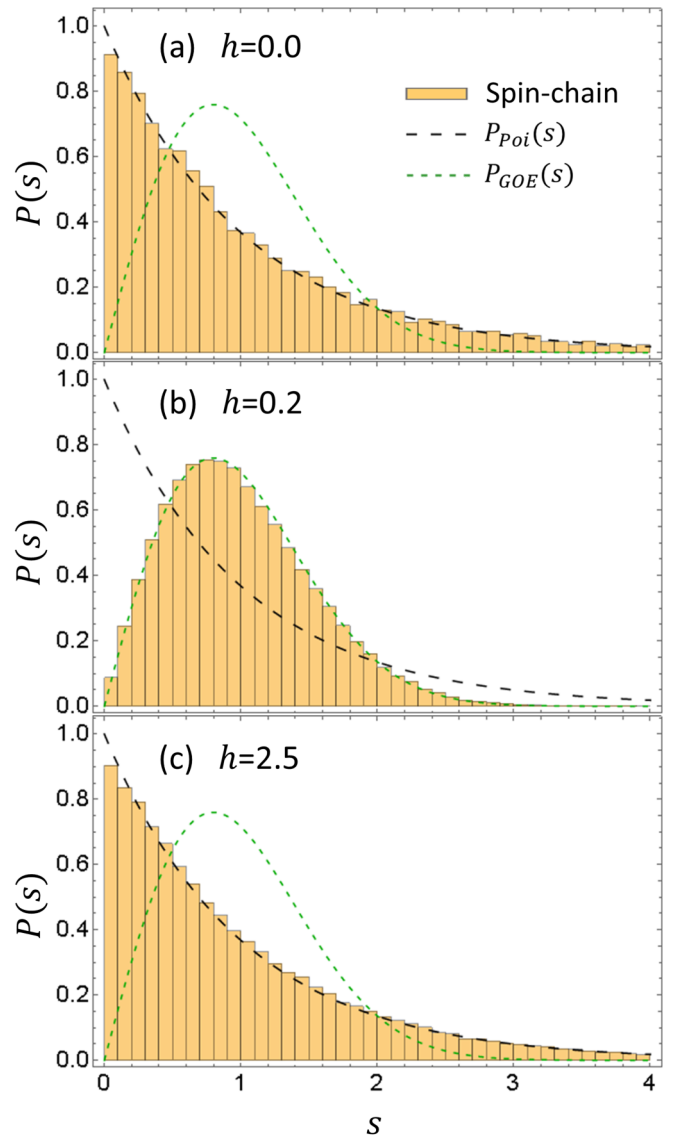

FIG. 1. NNSD for $N = 16$. (a) Shows Poissonian distribution when magnetic field is zero; (b) NNSD follows GOE for $h = 0.2$; and (c) shows how Poisson distribution is recovered due to eigenvector localization for a typical large magnetic field ($h = 2.5$).

crossover parameter h. We find that the best fits for $N = 14$, the above two extremes are obtained, respectively, for $\lambda = 0.013$ and 1.578, whereas for $N = 16$, the respective values are 0.013 and 1.507. Figures 3 and 4 show the corresponding plots.

2. GOE-to-GUE crossover

To realize GOE-to-GUE crossover we switch on the scalar chirality term in Eq. (1) by keeping the system in GOE regime, for which the value of h is fixed at 0.2 [see Figs. 1(b) and 2]. We can observe GOE-to-GUE crossover by slowly increasing the amplitude of scalar chirality term J_t. Again, to estimate the exact crossover points for the GOE-to-GUE crossover, we have used the KL divergence of $P(s)$ with respect to $P_{GUE}(s)$ and plotted D_{KL} against the symmetry-breaking physical crossover parameter J_t in Fig. 5. Here, the two extreme
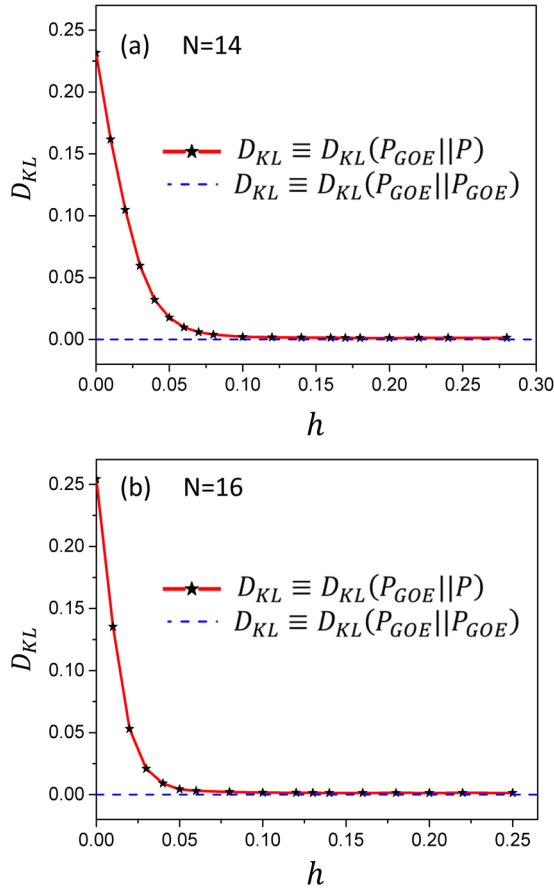
FIG. 2. Variation of $D_{\mathrm{KL}}(P_{\mathrm{GOE}}||P)$ [KL divergence of NNSD $P(s)$ with respect to $P_{\mathrm{GOE}}(s)$] with increasing value of the symmetry-breaking crossover parameter h for the (a) $N = 14$ and (b) $N = 16$ systems.
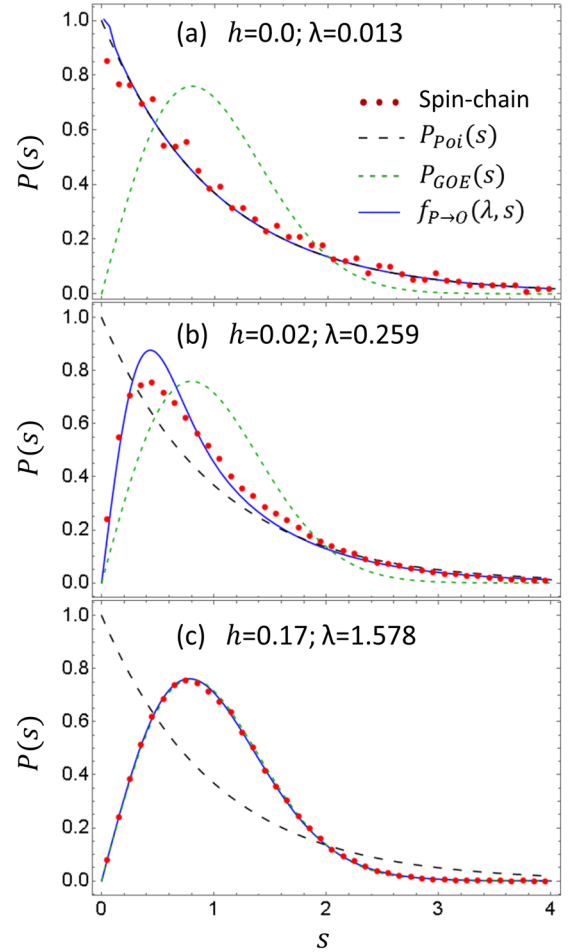

FIG. 3. NNSD for $N = 14$. Poissonian-to-GOE crossover with increasing h. (a), (c) Show the two limiting cases Poissonian and GOE, respectively and (b) shows one of the intermediate cases. We have used $f_{P \to O}(\lambda, s)$ to fit this crossover and the values of the RMT crossover parameter λ are determined.

cases correspond to GOE and GUE distributions for which KL divergence has a value ~ 0.047 [using the analytical forms $P_{\mathrm{GOE}}(s)$ and $P_{\mathrm{GUE}}(s)$, from Table I]. We observe in Fig. 5 that these extreme KL divergence values are 0.055 and 0.057 for $N = 14$ and 16 systems, respectively. While increasing J_t from zero, unlike the Poissonian-to-GOE crossover case, here we observe that some threshold amount of scalar spin-chirality amplitude (J_t) is needed to even start breaking the GOE symmetry (as indicated by the plateauing at low J_t), and further increment of J_t shows a linear variation with λ. For $N = 14$ and 16 systems, these threshold values are $(J_t)_{\mathrm{Th}} \sim 0.1$ and $(J_t)_{\mathrm{Th}} \sim 0.07$, respectively. The KL divergence saturates at around $J_t = 0.62$ and at around $J_t = 0.42$ for the $N = 14$ and 16 systems, respectively. So we claim that for these values the GOE-to-GUE crossover is complete. As we have kept h fixed at 0.2, we again conclude that with increasing system size, we can break the GOE symmetry of the system with lesser magnitude of scalar spin chirality and achieve the GUE distribution sooner.

Now, the GOE-to-GUE computed crossover data are mapped on to the interpolating function $f_{O \to U}(\lambda, s)$ of Eq. (5) and the values of RMT crossover parameter λ are noted against the physical crossover parameter J_t. We observe from Fig. 6 that in the GOE regime, the value of the RMT crossover

parameter λ is very close to zero, and at around $\lambda \sim 1.7$, $f_{O \to U}(\lambda, s)$ matches quite well with GUE distribution, for the $N = 14$ system (Fig. 6), and for the $N = 16$ system it achieves the GUE distribution for the RMT crossover value of $\lambda = 1.9$ (see Fig. 7, for details).

3. Crossovers using inverted spin basis

In this work, we are also interested in exploring the universality behavior of RMT spectral crossovers for our spin-chain systems, in the large system size limit. For this, we need to explore more than just two lattice sizes. This would also enable us to properly examine the existence of a universal scaling exponent (discussed in the next section). However, we have already pointed out the computational limitations to carry out calculations for systems beyond the lattice size $N = 16$. To circumvent this problem, we resort to a symmetry consideration to further reduce our system basis, as discussed below [118]. In our calculations we have used spin chains having even number of sites and, as discussed in detail earlier, restrict our calculations to the $\mathrm{S}^z = 0$ subspace. In this scenario, there exists a pair of equivalent basis vectors which
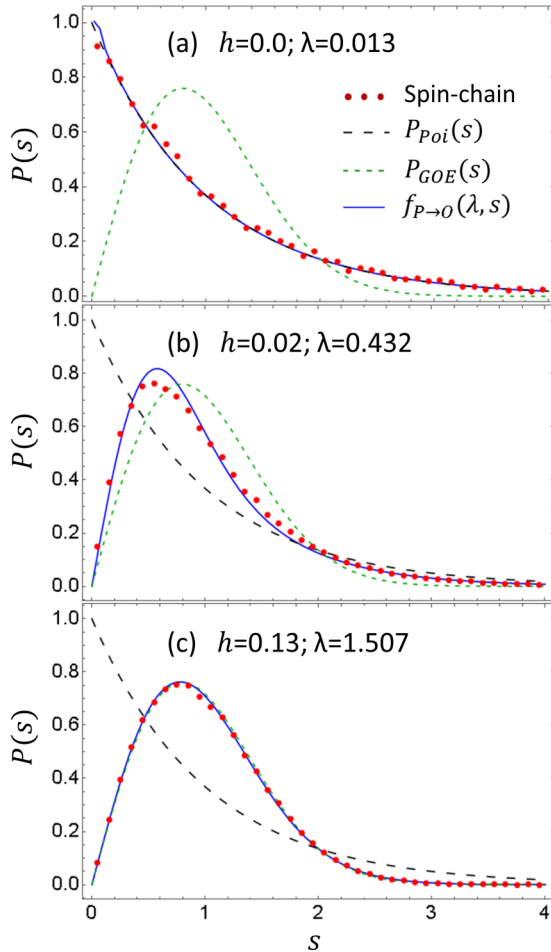
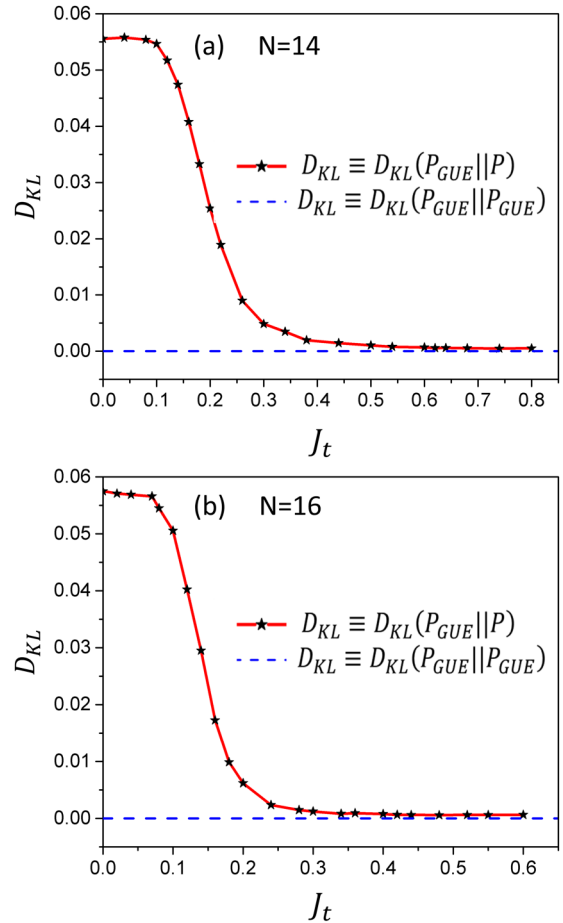FIG. 4. Plots of NNSD for $N = 16$, similar to the $N = 14$ cases in Fig. 3.

FIG. 5. Variation of $D_{KL}(P_{GUE}||P)$ [KL divergence of NNSD $P(s)$ with respect to $P_{GUE}(s)$] with the increasing value of symmetry-breaking crossover parameter J_t for (a) $N = 14$ and (b) $N = 16$ systems.

are related via global spin inversion [118]. If $|\downarrow\downarrow\uparrow\uparrow\downarrow\uparrow\rangle$ denotes a basis of six-site system having three up spin and three down spin, then the equivalent pair basis is denoted by the basis $|\uparrow\uparrow\downarrow\downarrow\uparrow\downarrow\rangle$. Now if we choose one basis vector out of each pair, then we have two subsets of basis vectors in the $S^z = 0$ subspace. We want to carry out NNSD calculations considering only one such subset and compare with the full basis results. In Figs. 8(a) and 8(b) we have plotted NNSD of $N = 14$ ($n = 1716$) and $N = 16$ ($n = 6435$) systems, considering $\mathcal{M} = 100$ and 20, respectively. We observe that the Poissonian-to-GOE crossovers take place around the same symmetry breaking h values when compared to the full basis calculations in Sec. IV A 1. We have also studied GOE-to-GUE crossovers in Figs. 9(a) and 9(b) for the $N = 14$ and 16 systems, respectively, and observed that the values of the physical crossover parameter J_t obtained from the inverted basis calculations are in good agreement with the results obtained from full basis calculations in Sec. IV A 2. The $N = 18$ system full basis ($n = 48\,620$) calculations are not possible due to computational limitations. However, in view of the above observations, we study the $N = 18$ system using inverted basis ($n = 24\,310$). For this, we consider $\mathcal{M} = 5$ and obtain the spacing distributions. These results are depicted in Figs. 8(c) and 9(c), where we find the Poissonian-to-GOE

crossover value for the $N = 18$ system is $h = 0.085$, and the GOE-to-GUE crossover takes place at around $J_t = 0.28$, for the same system, respectively. In the next sections, along with the $N = 14$ and 16 systems with $S^z = 0$ basis, we use the $N = 18$ system with inverted spin basis in all ratio distribution calculations and in universality studies.

4. Universality in NNSD

In the preceding subsections, we used the RMT interpolation functions based on 2×2 matrix models to fit the calculated data and obtained the crossover parameter λ. In order to investigate the universal aspects of RMT spectral crossovers, as discussed in the Introduction, we show that after suitable scaling of the physical parameters h and J_t, the crossovers are governed by identical values of the λ parameter for different lattice sizes, thereby establishing universality of the RMT crossover results. For the Poissonian-to-GOE crossover we plot the variation of the RMT interpolating parameter λ [of the crossover function $f_{P \to O}(\lambda, s)$] against the physical crossover parameter h in Fig. 10(a). Initially, it varies linearly with increasing magnetic field value, then it saturates as it approaches the GOE regime. We fit the linear part of this plot using a scaling function $n^a h$, where n is the dimension
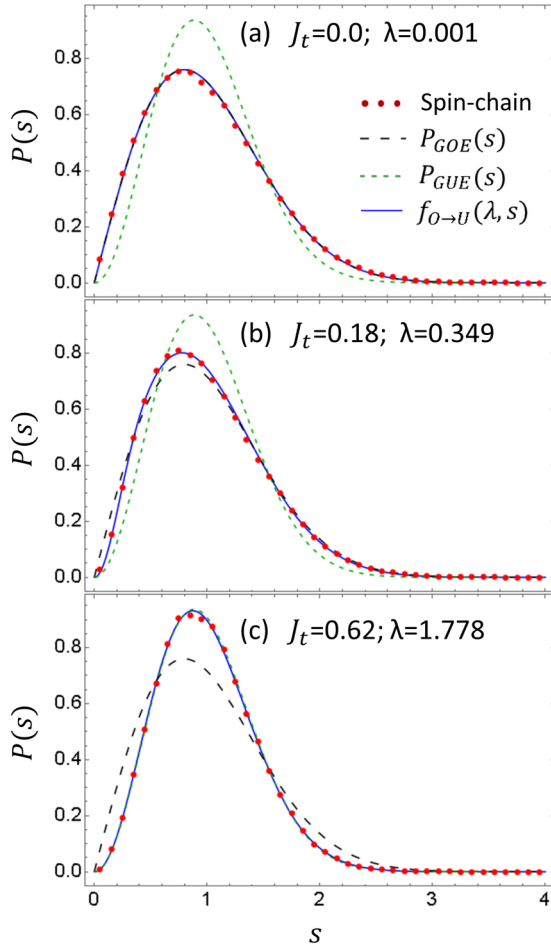
FIG. 6. NNSD for $N = 14$; GOE-to-GUE crossover with increasing scalar spin-chirality amplitude (J_t) by keeping the system at constant random magnetic field ($h = 0.2$). (a), (c) Show the two limiting cases GOE and GUE, respectively, and (b) shows one of the intermediate states. We have used $f_{O \to U}(\lambda, s)$ to fit this crossover and the value of the RMT crossover parameter λ is determined.
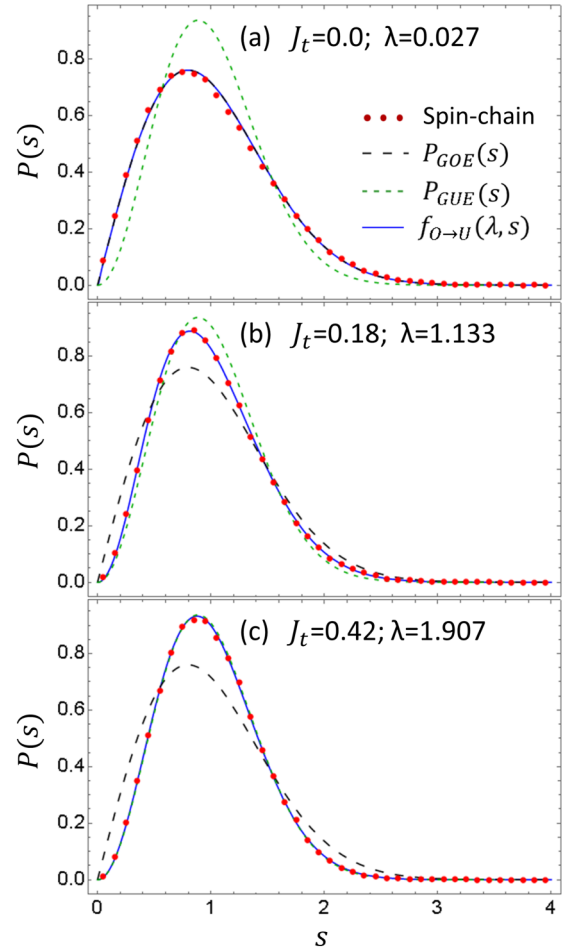
of the system Hamiltonian [$n = 3432$ for $N = 14$, $n = 12\,870$ for $N = 16$, and $n = 24\,310$ for $N = 18$ (inverted basis)] and a is the scaling exponent. In Fig. 10(b), λ is plotted against $n^a h$, the universal scaling exponent is found to be $a = 0.23$. Therefore, we conclude that we have found universality in the Poissonian-to-GOE crossover, in the large system size limit.

Similar behavior can be observed for the GOE-to-GUE crossover in Fig. 11(a), where we have plotted the variation of RMT interpolating parameter λ [of the crossover function $f_{O \to U}(\lambda, s)$] against the physical crossover parameter J_t. Again, we have fitted the linear increment part in Fig. 11(b) using the scaling function $n^a J_t$ and find that the universal scaling exponent a takes the value 0.25 [using $N = 14$, 16, and 18 (inverted basis) systems]. After the linear region, further increment of J_t saturates the crossover parameter λ into the GUE region. Thus, similar to the Poissonian-to-GOE crossover, here also we observe universality in the GOE $\rightarrow$ GUE crossover, in the large system size limit.

FIG. 7. Plots of NNSD for $N = 16$, similar to the $N = 14$ cases in Fig. 6.

B. Ratio distribution (RD)

We now examine the spacings-ratio distribution. To estimate the threshold of physical crossover parameters for which spectral crossovers are achieved, we have computed the KL divergence for NNSD. Similarly, we have studied the KL divergence for RD and find that the D_{KL} versus physical crossover parameter variations are not much different from NNSD. However, in the present case, it is interesting to study the average of the ratios $\langle r \rangle$ and $\langle \tilde{r} \rangle$, which also help classify the system in one regime or the other. It should be noted that such a study is not useful in the case of NNSD since the unfolding of eigenspectra necessarily makes the average spacing unity. The averages $\langle r \rangle = \int_0^\infty r \mathcal{P}(r) dr$ and $\langle \tilde{r} \rangle = \int_0^1 \tilde{r} \tilde{\mathcal{P}}(\tilde{r}) d\tilde{r}$ can be computed and the exact RMT values of these average ratios are included in Table III. We have calculated $\langle r \rangle$ and $\langle \tilde{r} \rangle$ for both the Poissonian-to-GOE and the GOE-to-GUE crossovers considering the $N = 14$, 16, and 18 systems. We have listed our calculated values of $\langle r \rangle$ and $\langle \tilde{r} \rangle$ at RMT crossovers for different ensembles in Table III.

At Poissonian limit, the exact RMT value $\langle r \rangle_{\mathrm{RMT}}$ is ∞ [96,114], but in practice we get relatively large finite values for our systems. The exact RMT value $\langle \tilde{r} \rangle_{\mathrm{RMT}}$ is 0.386 at Poissonian distribution and it is well in agreement with the calculated $\langle \tilde{r} \rangle$ values for our systems. We find that $\langle r \rangle$
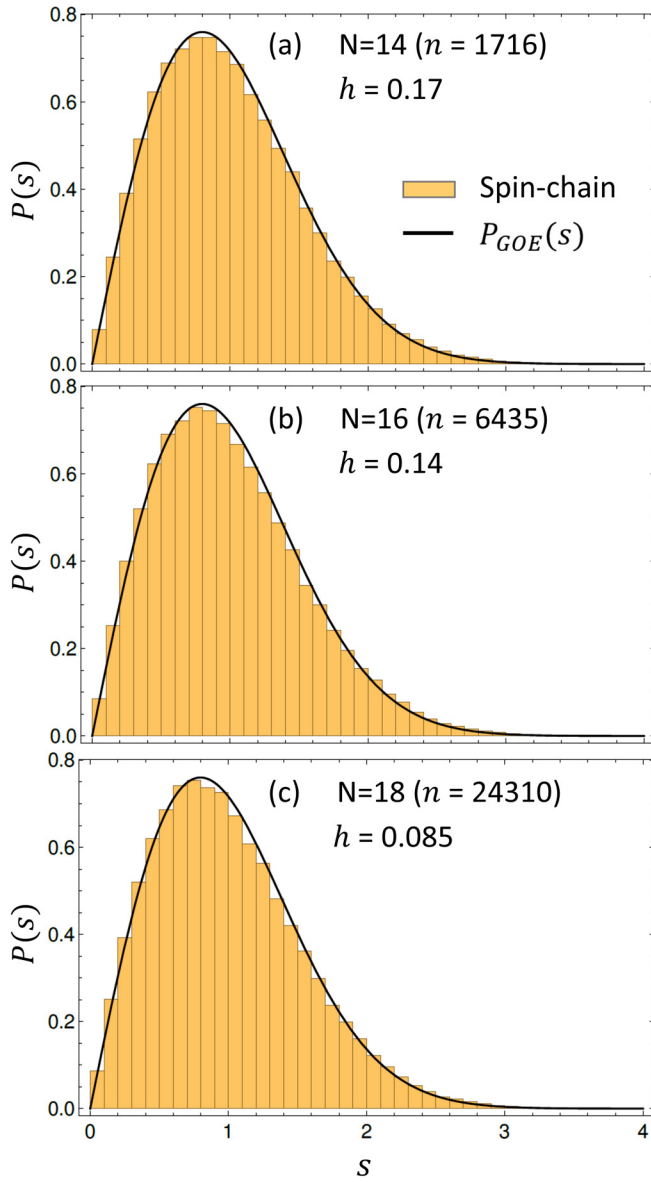
FIG. 8. Inverted basis GOE distribution for the (a) $N = 14$, (b) $N = 16$, and (c) $N = 18$ systems, at the crossover points.
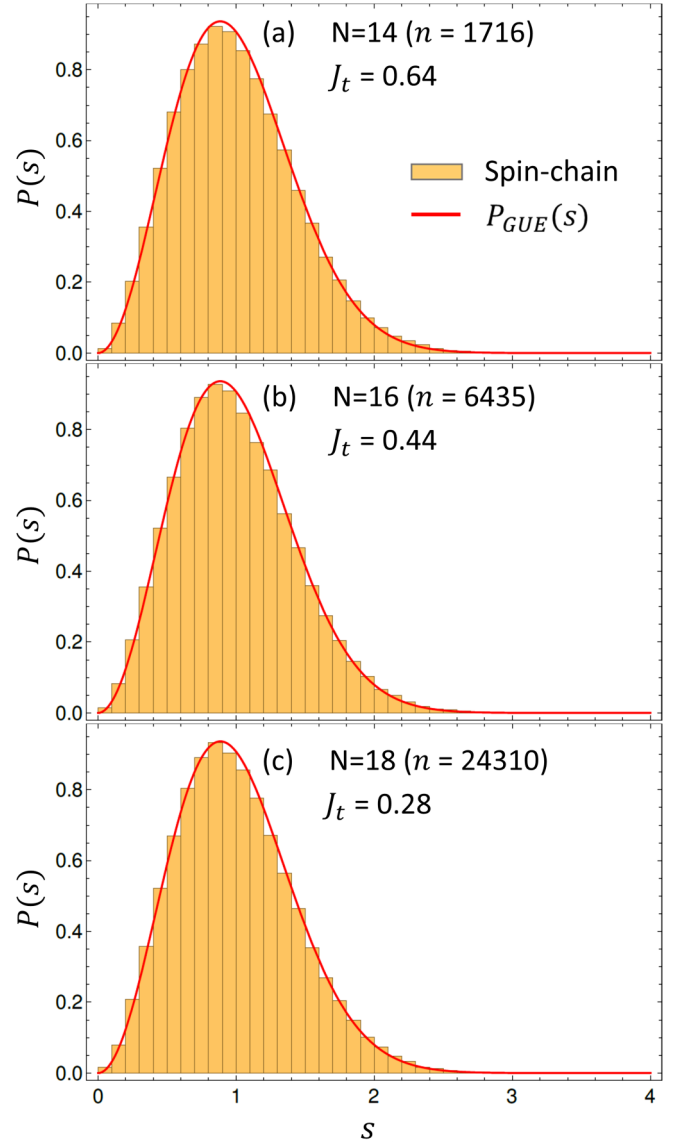

FIG. 9. Inverted basis GUE distribution for the (a) $N = 14$, (b) $N = 16$, and (c) $N = 18$ systems, at the crossover points.

TABLE III. Exact RMT values (from Refs. [96,114]) and the calculated (this work) values of $\langle r \rangle$ and $\langle \tilde{r} \rangle$.

Quantity	Poissonian	GOE	GUE
$\langle r \rangle_{\mathrm{RMT}}$	∞	1.750 1.800	1.361 1.376
$\langle r \rangle$	7.080 ($N = 14$) 11.41 ($N = 16$) 10.40 ($N = 18$)	1.772 ($N = 14$) 1.757 ($N = 16$) 1.755 ($N = 18$)	1.371 ($N = 14$) 1.372 ($N = 16$) 1.362 ($N = 18$)
$\langle \tilde{r} \rangle_{\mathrm{RMT}}$	0.386	0.536 0.528	0.603 0.598
$\langle \tilde{r} \rangle$	0.395 ($N = 14$) 0.385 ($N = 16$) 0.382 ($N = 18$)	0.531 ($N = 14$) 0.531 ($N = 16$) 0.530 ($N = 18$)	0.599 ($N = 14$) 0.599 ($N = 16$) 0.597 ($N = 18$)

achieves the values 1.772 ($h = 0.17$), 1.757($h = 0.13$), and 1.755 ($h = 0.085$) in the GOE regime for $N = 14$, 16, and 18 systems, respectively, against the RMT values listed in Table III. Please see the Supplemental Material for a detailed variation of $\langle r \rangle$ and $\tilde{r}$ with h and J_t [119]. Our systems saturate to the GUE regime at around $\langle r \rangle = 1.37$ ($\langle \tilde{r} \rangle = 0.599$) for $N = 14$ and 16 and at 1.36 (0.597) for $N = 18$. Our spin-chain model conforms to different RMT symmetry classes with the variation of physical crossover parameters h and J_t, and the calculated values of $\langle r \rangle$ and $\langle \tilde{r} \rangle$ are in good agreement with the theoretical RMT values $\langle r \rangle_{\mathrm{RMT}}$ and $\langle \tilde{r} \rangle_{\mathrm{RMT}}$ [96,114].

1. Poissonian-to-GOE and GOE-to-GUE crossovers in ratio distribution

To study the Poissonian [$\mathcal{P}_{\mathrm{Poi}}(r)$] to GOE [$\mathcal{P}_{\mathrm{GOE}}(r)$] crossover in the ratio distribution for our spin-chain model [Eq. (1)], we plot $\mathcal{P}(r)$ versus r in Figs. 12, 13, and 14, for the $N = 14$, 16, and 18 systems, respectively. We observe that
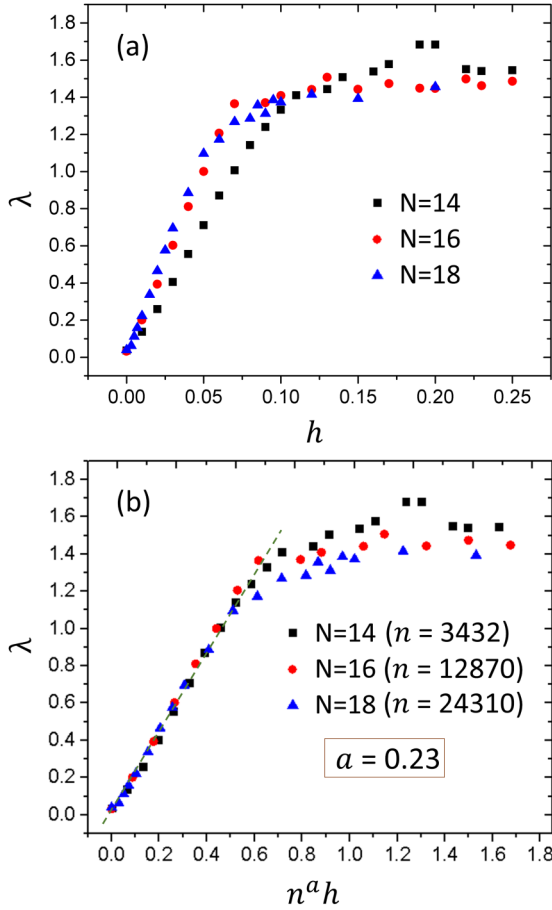
FIG. 10. Variation of RMT crossover parameter λ [of the crossover function $f_{P \to O}(\lambda, s)$] with (a) physical crossover parameter h, for the $N = 14$, 16, and 18 (inverted basis) systems. Poissonian-to-GOE crossover is observed when λ gets saturated, for $N = 14$ the crossover value is $h = 0.17$, for $N = 16$ it is $h = 0.13$, and for $N = 18$ it is $h = 0.085$. (b) The coinciding linear region of the plots is fitted with the scaling function $n^a h$. λ is plotted against $n^a h$. The universal scaling exponent $a = 0.23$. The dashed green line is a fit based on the data points occurring in the linear regime.

FIG. 11. Variation of RMT crossover parameter λ [of the crossover function $f_{O \to U}(\lambda, s)$] with (a) physical crossover parameter J_t for $N = 14$, 16, and 18 (inverted basis) systems. GOE-to-GUE crossover is observed when λ gets saturated, for $N = 14$ the crossover value is $J_t = 0.62$, for $N = 16$ it is $J_t = 0.42$, and for $N = 18$ it is $J_t = 0.28$. (b) The coinciding linear region of the plots is fitted with the scaling function $n^a J_t$. λ is plotted against $n^a J_t$. The universal scaling exponent $a = 0.25$. The dashed green line is a fit based on the data points occurring in the linear regime.

for the $N = 14$ system, the $\mathcal{P}(r)$ histogram follows $\mathcal{P}_{GOE}(r)$ at $h = 0.16$ whereas, for the $N = 16$ and 18 systems the computed ratio distribution matches $\mathcal{P}_{GOE}(r)$ at around $h = 0.11$ and 0.09, respectively. These values for the crossover points observed from NNSD are quite comparable with those obtained from the ratio distribution results.

By keeping the spin-chain model well inside the GOE regime ($h = 0.20$) we study the GOE [$\mathcal{P}_{GOE}(r)$] to GUE [$\mathcal{P}_{GUE}(r)$] crossover in the ratio distribution for the $N = 14$ (Fig. 15), $N = 16$ (Fig. 16), and $N = 18$ (Fig. 17) systems. The observed values of scalar chirality parameter J_t at the GUE crossover in ratio distribution match quite well with the NNSD findings, being at $J_t = 0.62$, 0.42, and 0.28 for the $N = 14$, 16, and 18 systems, as seen from Figs. 15, 16, and 17, respectively.

For the Poissonian-to-GOE crossover, there is no analytical expression available for the ratio distribution interpolating function which can be compared with our observed results from spin chains. Therefore, we simulate the Poissonian-to-
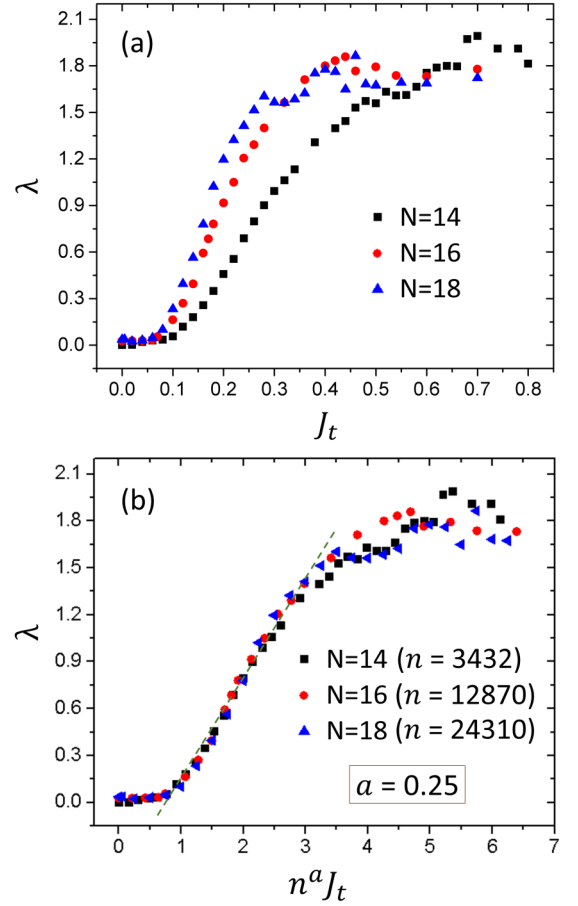
GOE crossover using the Pandey-Mehta crossover Hamiltonian, as described in Eq. (3), using 3×3 matrices $\mathcal{H}_0$ and $\mathcal{H}_\infty$ taken from the Poissonian and the Gaussian orthogonal ensembles, respectively. The crossover is realized by varying λ from 0 to relatively large numerical values. We calculate the probability distribution of ratios of the eigenvalue spacings for the matrix $\mathcal{H}$ and denote it by $\mathcal{E}_{P \to O}(\lambda, r)$. We show in Figs. 12–14 that $\mathcal{E}_{P \to O}(\lambda, r)$ can interpolate between the Poissonian-to-GOE crossover quite accurately for our systems.

For the GOE-to-GUE crossover, analytical expression for the interpolating function $\mathcal{F}_{O \to U}(\lambda, r)$ [Eq. (6)] is available. We use it to map the GOE-to-GUE crossover in our spin-chain model onto a RMT description. This function interpolates the crossover perfectly for all the systems (Figs. 15–17).

The simulated interpolating probability distribution $\mathcal{E}_{P \to O}(\lambda, r)$ and the analytical interpolating function $\mathcal{F}_{O \to U}(\lambda, r)$ are based on 3×3 matrix ensembles. But by applying these to a physical system here, we have
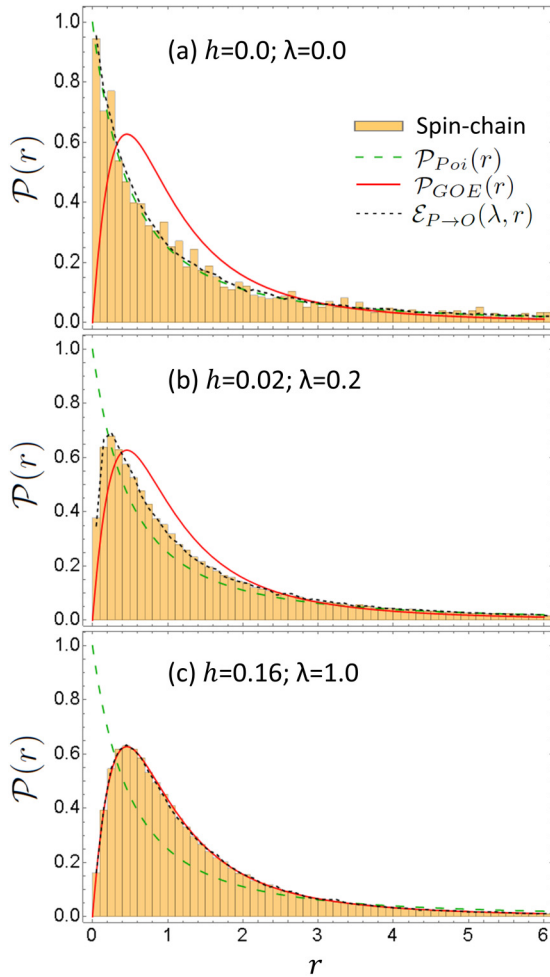
FIG. 12. (a) Poissonian → (b) intermediate → (c) GOE crossover for probability distribution of ratios with the increasing value of h for the $N = 14$ system.

FIG. 13. (a) Poissonian → (b) intermediate → (c) GOE crossover for probability distribution of ratios with the increasing value of h for the $N = 16$ system.

successfully shown that, similar to Wigner surmises, they can be used for much higher-dimensional matrices, relevant for realistic physical systems, too.

2. Universality in ratio distribution

In this section we study the universality aspects of both the crossovers in the ratio distribution. In the last section we studied the crossovers in the ratio distribution $\mathcal{P}(r)$ with varying physical crossover parameters h and J_t. Here we have explored the variation of the generic RMT crossover parameter λ, against the physical crossover parameters in the ratio distribution. The Poissonian-to-GOE crossover in our system is interpolated quite accurately by the $\mathcal{E}_{P \to O}(\lambda, r)$ distribution, with increasing λ. In Fig. 18 we plot the variation of λ with the physical crossover parameter h scaled with n^a. We observe the emergence of universality in the Poissonian-to-GOE crossover in the ratio distribution, for large system sizes. The universal scaling exponent a here assumes the value of 0.25, which is quite comparable to the corresponding universal scaling exponent of NNSD, where it has a value of 0.23.

Since the ratio distribution for the GOE-to-GUE crossover in our system is properly interpolated by the RMT interpolat-
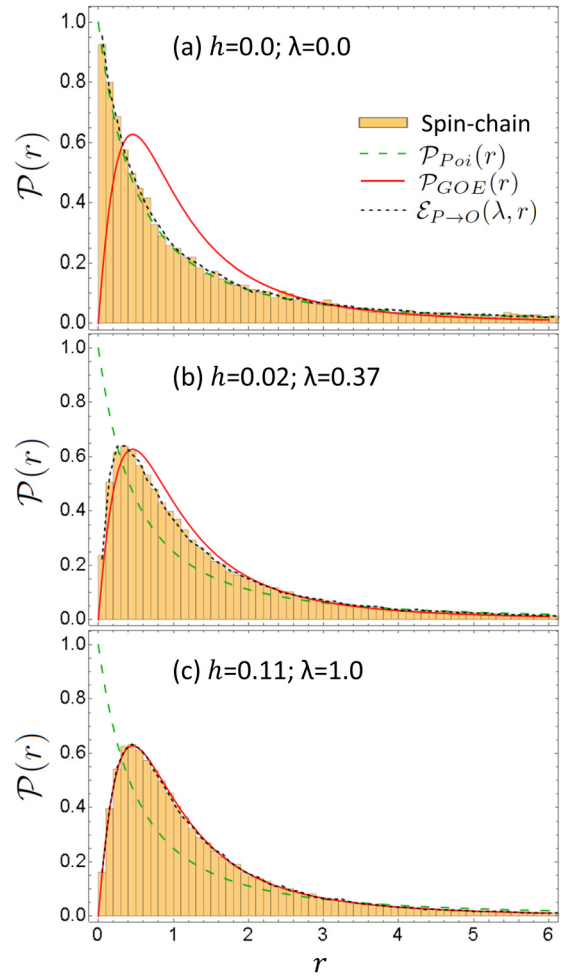
ing function $\mathcal{F}_{O \to U}(\lambda, r)$ with increasing λ, so we study the variation of λ with the scaled physical crossover parameter $n^a J_t$ in Fig. 19. The universality of the GOE-to-GUE crossover in the ratio distribution is observed in Fig. 19 and the universal scaling exponent comes out to be $a = 0.26$. This is very close to the universal exponent of 0.25, observed in NNSD, pointing towards a universality in the value of the scaling exponent itself.

V. CONCLUSIONS

We have studied the eigenvalue statistics and spectral crossovers between different RMT symmetry classes (Poissonian → GOE and GOE → GUE), for one-dimensional quantum spin chains with multispin interactions, coupled to random, inhomogeneous magnetic fields, as various symmetries are gradually broken by tuning of suitable physical parameters. We have focused on its correspondence with the corresponding crossovers in exact RMT models, as embodied in the NNSD (which captures a two-point spectral correlation) and the RD (which reflects a three-point spectral correlation). We find an excellent one-to-one correspondence between the RMT results and the properties of the physical spin systems,
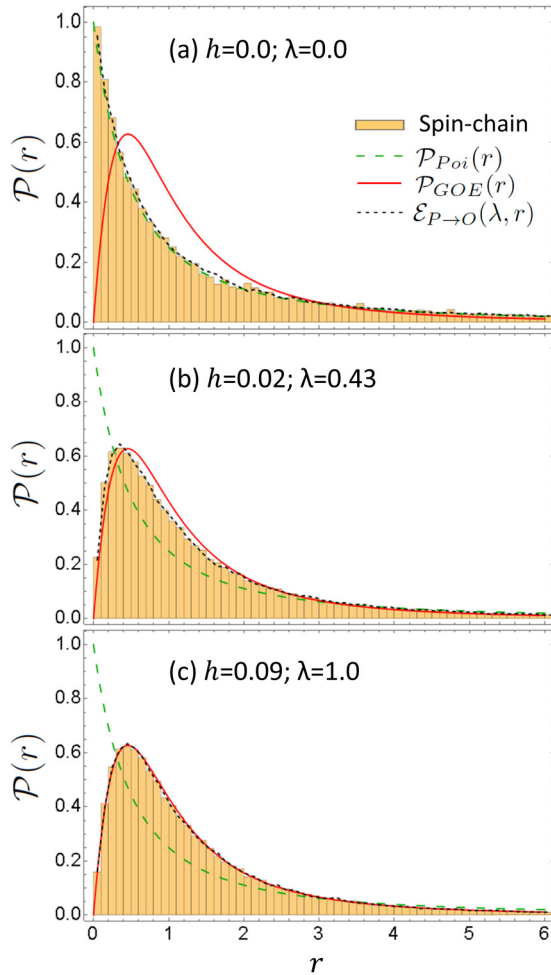
FIG. 14. (a) Poissonian → (b) intermediate → (c) GOE crossover for probability distribution of ratios with the increasing value of h for the $N = 18$ system.
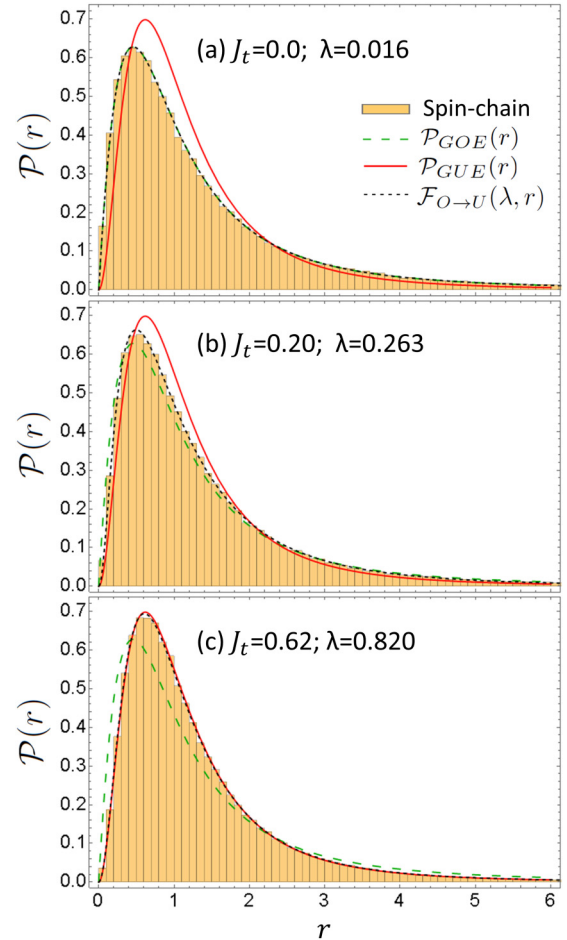

FIG. 15. Ratio distribution for $N = 14$; (a)–(c) Show the GOE-to-GUE crossover with the increasing value of physical crossover parameter J_t, while the value of the range of the random magnetic field (h) is kept at 0.2. $\mathcal{F}_{O \to U}(\lambda, r)$ interpolates this crossover properly.

which points towards the robustness of the RMT formalism and the Wigner-Dyson-Berry-Tabor classification, as also encountered in many other physical systems [30–36,90–94]. We summarize below some salient conclusions from this detailed study:

(1) To obtain a good description in terms of RMT results, one needs relatively large lattice sizes, which luckily saturate soon enough by $N = 18$. One also finds that the symmetry is broken by progressively smaller symmetry-breaking physical parameters, as the system size is increased.

(2) Using a finite-size scaling analysis we have uncovered a universality in these crossovers. There are two facets to this. *First*, by suitably scaling the physical crossover parameter by the Hamiltonian basis size raised to the power of a suitable scaling exponent (a), in each type of crossover, one is able to collapse the RMT scaling parameter (λ) versus the physical scaling parameter plots for various lattice sizes, onto one universal plot. *Second*, irrespective to the type of crossover (Poissonian → GOE, or GOE → GUE) or the spectral correlation measure used (i.e., NNSD or RD), the scaling exponent (a) seems to hover around the value of ~ 0.25 (between 0.23–

0.26). Interestingly, the value of this exponent seems to be quite robust too.

(3) For this kind of investigation, the many-body basis size grows very fast with the lattice size, in spite of restricting to the smallest S^z sector. Moreover, the exact diagonalization process needs to be repeated a large number of times, as physical parameters have to be continuously varied over a sizable range to capture the crossovers and also for configuration (ensemble) averaging over the random magnetic field. To add to the problem, one typically needs *all* eigenvalues, and so one cannot rely on iterative diagonalization schemes like the Lanczos method to reduce computational costs as they yield only extremal eigenvalues and eigenstates. The only saving grace is the use of additional symmetries and we have demonstrated here the usefulness of one such symmetry, viz., global spin-rotational symmetry to truncate to an *inverted basis*, that reduces the basis size to half its original value.

Future directions could involve extending these methods to study higher-dimensional correlated spin models, long-range spectral fluctuations, or generalization to fermionic models, etc. Some of these investigations are already under way.
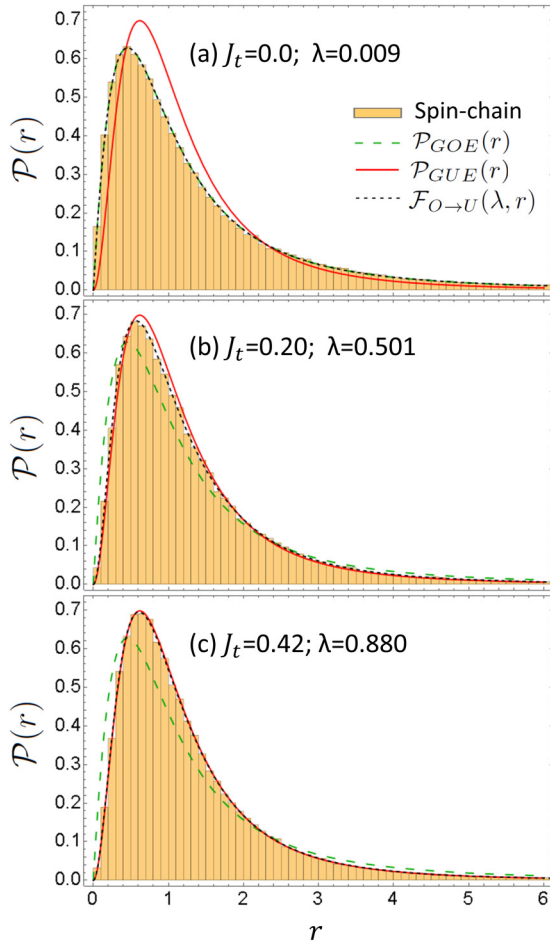
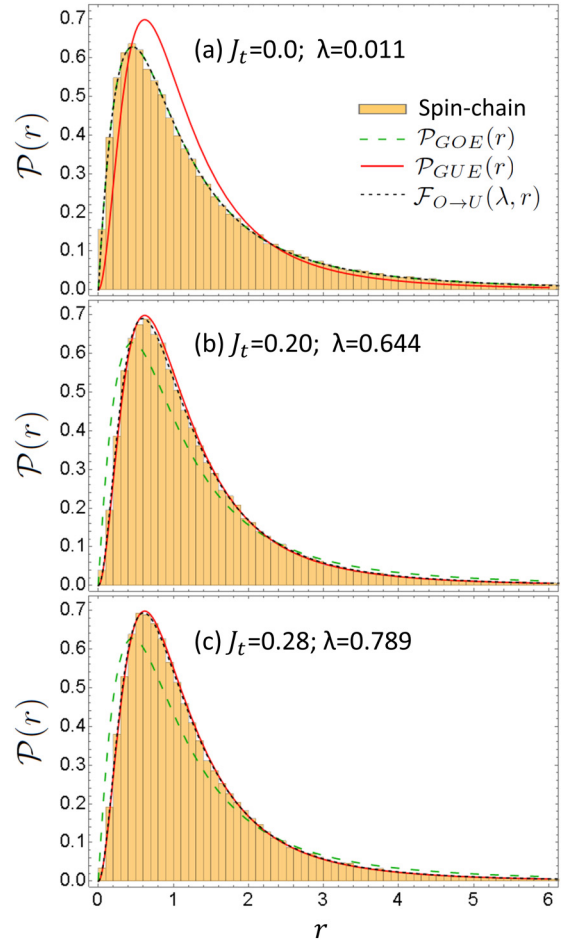FIG. 16. Ratio distribution for the $N = 16$ system, similar to the $N = 14$ cases in Fig. 15.

FIG. 17. Ratio distribution for the $N = 18$ system, similar to the $N = 14$ cases in Fig. 15.

APPENDIX: SIMPLIFICATION OF THE SCALAR SPIN-CHIRALITY TERM

This Appendix presents a compact derivation of Eq. (2). Einstein summation convention is used throughout this section. We have

$$\mathbf{S}_j \cdot [\mathbf{S}_{j+1} \times \mathbf{S}_{j+2}] = \mathbf{S}_j \cdot \mathbf{S}_c = S_j^\alpha S_c^\alpha$$

$$= \varepsilon_{\alpha\beta\gamma} S_j^\alpha S_{(j+1)}^\beta S_{(j+2)}^\gamma. \qquad (A1)$$

Here, α, β, and γ run over the spin components (x, y, z). As we know exchanging rows and columns leaves a determinant unchanged, we obtain

$$\varepsilon_{\alpha\beta\gamma} S_j^\alpha S_{(j+1)}^\beta S_{(j+2)}^\gamma = \begin{vmatrix} S_j^x & S_j^y & S_j^z \\ S_{(j+1)}^x & S_{(j+1)}^y & S_{(j+1)}^z \\ S_{(j+2)}^x & S_{(j+2)}^y & S_{(j+2)}^z \end{vmatrix}$$
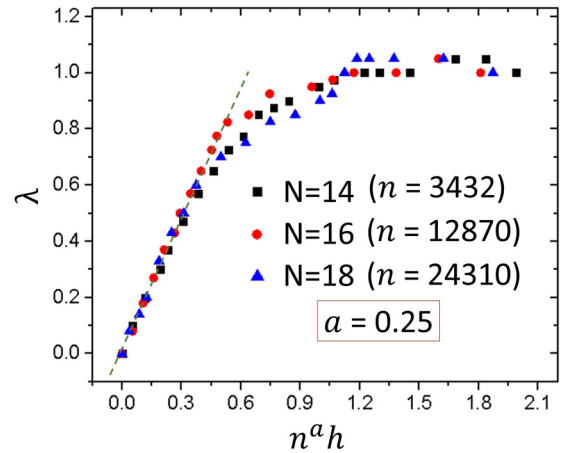

FIG. 18. Scaling in ratio distribution for the Poissonian-to-GOE crossover. λ of the interpolating matrix model's level-spacing ratio distribution $\mathcal{E}_{P \to O}(\lambda, r)$ is plotted against the scaled physical crossover parameter h. Here the universal scaling exponent $a = 0.25$. The dashed green line is a fit based on the data points occurring in the linear regime.
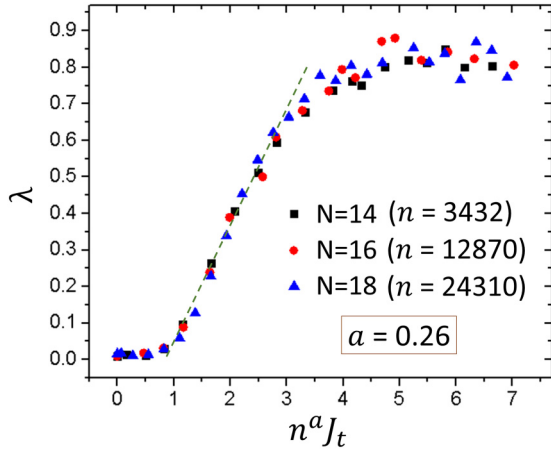
FIG. 19. Scaling in ratio distribution for the GOE-to-GUE crossover. λ of the interpolating function $\mathcal{F}_{O\to U}(\lambda, r)$ is plotted against the scaled physical crossover parameter J_t. Here the universal scaling exponent $a = 0.26$. The dashed green line is a fit based on the data points occurring in the linear regime.

$$= \begin{vmatrix} S_j^x & S_{(j+1)}^x & S_{(j+2)}^x \\ S_j^y & S_{(j+1)}^y & S_{(j+2)}^y \\ S_j^z & S_{(j+1)}^z & S_{(j+2)}^z \end{vmatrix}$$

$$= \varepsilon_{klm} S_k^x S_l^y S_m^z, \qquad (A2)$$

where $k = j$, $l = j + 1$, and $m = j + 2$. With this the Levi-Civita indices now run over sites rather than spin components (x, y, z).

The spin components are related to spin ladder operators as

$$S^x = \frac{1}{2}(S^+ + S^-), \quad S^y = \frac{1}{2i}(S^+ - S^-). \qquad (A3)$$

Now, using Eq. (A3) we get

$$\varepsilon_{klm} S_k^x S_l^y S_m^z = \frac{1}{4i}\big[\varepsilon_{klm} S_k^+ S_l^+ S_m^z - \varepsilon_{klm} S_k^- S_l^- S_m^z$$
$$- \varepsilon_{klm} S_k^+ S_l^- S_m^z + \varepsilon_{klm} S_k^- S_l^+ S_m^z\big]. \quad (A4)$$

The first term leads to

$$\varepsilon_{klm} S_k^+ S_l^+ S_m^z = -\varepsilon_{lkm} S_k^+ S_l^+ S_m^z$$
$$= -\varepsilon_{lkm} S_l^+ S_k^+ S_m^z = -\varepsilon_{klm} S_k^+ S_l^+ S_m^z, \qquad (A5)$$

where in the second step we have used the commutation relation $[S_k^+, S_l^+] = 0$ between distinct sites, and in the last step we have exchanged the dummy indices k and l. Thus, it follows that

$$\varepsilon_{klm} S_k^+ S_l^+ S_m^z = 0.$$

Similarly, we have

$$\varepsilon_{klm} S_k^- S_l^- S_m^z = 0.$$

Now, the third term of Eq. (A4) leads to

$$-\varepsilon_{klm} S_k^+ S_l^- S_m^z = \varepsilon_{lkm} S_k^+ S_l^- S_m^z$$
$$= \varepsilon_{lkm} S_l^- S_k^+ S_m^z = \varepsilon_{klm} S_k^- S_l^+ S_m^z,$$

where in the second step we have used the commutation relation $[S_k^+, S_l^-] = 0$ because the Levi-Civita symbol ensures that k and l always assume distinct site values, and in the last step we have exchanged the dummy indices k and l. So, Eq. (A4) becomes

$$\varepsilon_{klm} S_k^x S_l^y S_m^z = \frac{1}{4i} 2\varepsilon_{klm} S_k^- S_l^+ S_m^z$$
$$= \frac{-i}{2}\varepsilon_{klm} S_k^- S_l^+ S_m^z = \frac{i}{2}\varepsilon_{mlk} S_m^z S_k^- S_l^+$$
$$= \frac{i}{2}\varepsilon_{mlk} S_m^z S_l^+ S_k^- = \frac{i}{2}\varepsilon_{klm} S_k^z S_l^+ S_m^-,$$

where the names of dummy indices have just been interchanged. This establishes Eq. (2).

[1] J. Hubbard, Proc. R. Soc. Lond. A **276**, 238 (1963).

[2] P. Fazekas, *Lecture Notes on Electron Correlation and Magnetism* (World Scientific, Singapore, 1999).

[3] E. H. Lieb, *The Hubbard Model* (Springer, New York, 1995).

[4] G. D. Mahan, *Many-Particle Physics* (Springer, New York, 2000).

[5] P. W. Anderson, Phys. Rev. **79**, 350 (1950).

[6] P. W. Anderson, Phys. Rev. **115**, 2 (1959).

[7] P. W. Anderson, *A Career in Theoretical Physics* (World Scientific, Singapore, 1994).

[8] K. I. Kugel and D. I. Khomskii, Usp. Fiz. Nauk **136**, 621 (1982) [Sov. Phys.–Usp. **25**, 231 (1982)].

[9] G. Khaliullin and V. Oudovenko, Phys. Rev. B **56**, R14243 (1997).

[10] T. Moriya, Phys. Rev. Lett. **4**, 228 (1960).

[11] T. Moriya, Phys. Rev. **120**, 91 (1960).

[12] I. E. Dzialoshinskii, Zh. Eksp. Teor. Fiz. **32**, 1547 (1957) [J. Exp. Theor. Phys. **5**, 1259 (1957)]; I. Dzyaloshinsky, J. Phys. Chem. Solids **4**, 241 (1958).

[13] X. G. Wen, F. Wilczek, and A. Zee, Phys. Rev. B **39**, 11413 (1989).

[14] D. S. Rokhsar, Phys. Rev. Lett. **65**, 1506 (1990).

[15] J. K. Freericks, L. M. Falicov, and D. S. Rokhsar, Phys. Rev. B **44**, 1458 (1991).

[16] D. Sen and R. Chitra, Phys. Rev. B **51**, 1922 (1995).

[17] P. W. Anderson, Phys. Rev. **124**, 41 (1961).

[18] E. Abrahams, P. W. Anderson, D. C. Licciardello, and T. V. Ramakrishnan, Phys. Rev. Lett. **42**, 673 (1979).

[19] P. W. Anderson, D. J. Thouless, E. Abrahams, and D. S. Fisher, Phys. Rev. B **22**, 3519 (1980).

[20] A. Lagendijk, B. v. Tiggelen, and D. S. Wiersma, Phys. Today **62**(8), 24 (2009).

[21] A. L. Efros and B. I. Shklovskii, J. Phys. C: Solid State Phys. **8**, L49 (1975).

[22] R. A. Römer and A. Punnoose, Phys. Rev. B **52**, 14809 (1995).

[23] A. Punnoose and A. M. Finkel'stein, Science **310**, 289 (2005).

[24] A. Punnoose and A. M. Finkel'stein, Phys. Rev. Lett. **96**, 057202 (2006).

[25] M. Mehta, *Random Matrices*, Pure and Applied Mathematics (Elsevier, Amsterdam, 2004).

[26] F. Haake, S. Gnutzmann, and M. Kuś, *Quantum Signatures of Chaos*, 4th ed. (Springer, Cham, 2018).

[27] T. Guhr, A. Muller-Groeling, and H. A. Weidenmuller, Phys. Rep. **299**, 189 (1998).

[28] P. J. Forrester, *Log-Gases and Random Matrices (LMS-34)*, Vol. 34 (Princeton University Press, Princeton, NJ, 2010).

[29] *Handbook of Random Matrix Theory*, edited by G. Akemann, J. Baik, and P. D. Francesco (Oxford University Press, Oxford, 2011).

[30] Y. Avishai, J. Richert, and R. Berkovits, Phys. Rev. B **66**, 052416 (2002).

[31] R. Modak and S. Mukerjee, New J. Phys. **16**, 093016 (2014).

[32] A. Y. Abul-Magd and M. H. Simbel, Phys. Rev. E **60**, 5371 (1999).

[33] N. Chavda and V. Kota, Phys. Lett. A **377**, 3009 (2013).

[34] C. L. Bertrand and A. M. García-García, Phys. Rev. B **94**, 144201 (2016).

[35] S. Iyer, V. Oganesyan, G. Refael, and D. A. Huse, Phys. Rev. B **87**, 134202 (2013).

[36] M. Collura, H. Aufderheide, G. Roux, and D. Karevski, Phys. Rev. A **86**, 013615 (2012).

[37] F. J. Dyson, J. Math. Phys. **3**, 1199 (1962).

[38] E. P. Wigner, Proc. Cambridge Philos. Soc. **47**, 790 (1951).

[39] C. E. Porter (ed.), *Statistical Theories of Spectra: Fluctuations* (Academic, New York, 1965).

[40] E. P. Wigner, *Statistical Properties of Real Symmetric Matrices with Many Dimensions* (Princeton University Press, Princeton, NJ, 1957), pp. 188–198.

[41] M. Mehta, Nucl. Phys. **18**, 395 (1960).

[42] V. Plerou, P. Gopikrishnan, B. Rosenow, L. A. Nunes Amaral, and H. E. Stanley, Phys. Rev. Lett. **83**, 1471 (1999).

[43] M. S. Santhanam and P. K. Patra, Phys. Rev. E **64**, 016102 (2001).

[44] P. Seba, Phys. Rev. Lett. **91**, 198104 (2003).

[45] E. Wigner, Phys. Rev. **40**, 749 (1932).

[46] E. P. Wigner, Ann. Math. **62**, 548 (1955).

[47] E. P. Wigner, Ann. Math. **65**, 203 (1957).

[48] E. P. Wigner, Ann. Math. **67**, 325 (1958).

[49] F. J. Dyson, J. Math. Phys. **3**, 140 (1962).

[50] L. F. Santos and M. Rigol, Phys. Rev. E **81**, 036206 (2010).

[51] M. Rigol and L. F. Santos, Phys. Rev. A **82**, 011604(R) (2010).

[52] C. Kollath, G. Roux, G. Biroli, and A. M. Lauchli, J. Stat. Mech.: Theory Exp. (2010) P08011.

[53] L. F. Santos, F. Borgonovi, and F. M. Izrailev, Phys. Rev. Lett. **108**, 094102 (2012).

[54] L. D'Alessio, Y. Kafri, A. Polkovnikov, and M. Rigol, Adv. Phys. **65**, 239 (2016).

[55] M. V. Berry, M. Tabor, and J. M. Ziman, Proc. R. Soc. London, Ser. A **356**, 375 (1977).

[56] O. Bohigas, M. J. Giannoni, and C. Schmit, Phys. Rev. Lett. **52**, 1 (1984).

[57] J.-S. Caux and J. Mossel, J. Stat. Mech.: Theory Exp. (2011) P02023.

[58] J. L. Lebowitz and O. Penrose, Phys. Today **26**(2), 23 (1973).

[59] O. Penrose, Rep. Prog. Phys. **42**, 1937 (1979).

[60] G. Gallavotti, *Statistical Mechanics*, 1st ed. (Springer, Berlin, 1999), pp. XIV, 342.

[61] M. Srednicki, Phys. Rev. E **50**, 888 (1994).

[62] M. Rigol, V. Dunjko, and M. Olshanii, Nature (London) **452**, 854 (2008).

[63] B. S. Shastry, Phys. Rev. Lett. **56**, 1529 (1986).

[64] M. Rigol, V. Dunjko, V. Yurovsky, and M. Olshanii, Phys. Rev. Lett. **98**, 050405 (2007).

[65] J. M. Deutsch, Phys. Rev. A **43**, 2046 (1991).

[66] M. Rigol, Phys. Rev. Lett. **103**, 100403 (2009).

[67] F. J. Dyson and M. L. Mehta, J. Math. Phys. **4**, 701 (1963).

[68] V. Lopac, I. Mrkonjić, and D. Radić, Phys. Rev. E **59**, 303 (1999).

[69] V. K. B. Kota, *Embedded Random Matrix Ensembles in Quantum Physics* (Springer, Cham, 2014).

[70] A. M. García-García, Y. Jia, D. Rosa, and J. J. M. Verbaarschot, Phys. Rev. D **103**, 106002 (2021).

[71] F. J. Dyson, J. Math. Phys. **3**, 1191 (1962).

[72] G. Lenz and F. Haake, Phys. Rev. Lett. **67**, 1 (1991).

[73] N. Chavda, H. Deota, and V. Kota, Phys. Lett. A **378**, 3012 (2014).

[74] R. Modak, S. Mukerjee, and S. Ramaswamy, Phys. Rev. B **90**, 075152 (2014).

[75] A. Sarkar, M. Kothiyal, and S. Kumar, Phys. Rev. E **101**, 012216 (2020).

[76] S. Kumar and A. Pandey, Phys. Rev. E **79**, 026211 (2009).

[77] S. Kumar and A. Pandey, Ann. Phys. **326**, 1877 (2011).

[78] A. Pandey and M. L. Mehta, Commun. Math. Phys. **87**, 449 (1983).

[79] M. L. Mehta and A. Pandey, J. Phys. A: Math. Gen. **16**, 2655 (1983).

[80] F. Schweiner, J. Main, and G. Wunner, Phys. Rev. E **95**, 062205 (2017).

[81] V. K. B. Kota and S. Sumedha, Phys. Rev. E **60**, 3405 (1999).

[82] S. H. Tekur, S. Kumar, and M. S. Santhanam, Phys. Rev. E **97**, 062212 (2018).

[83] A. Pandey, Chaos Solitons Fractals **5**, 1275 (1995).

[84] C. W. J. Beenakker, Rev. Mod. Phys. **69**, 731 (1997).

[85] E. P. Wigner, SIAM Rev. **9**, 1 (1967).

[86] J. B. French and V. K. B. Kota, Annu. Rev. Nucl. Part. Sci. **32**, 35 (1982).

[87] G. Lenz, K. Życzkowski, and D. Saher, Phys. Rev. A **44**, 8043 (1991).

[88] E. Caurier, B. Grammaticos, and A. Ramani, J. Phys. A: Math. Gen. **23**, 4903 (1990).

[89] A. Pandey, Ann. Phys. **134**, 110 (1981).

[90] J. French, V. Kota, A. Pandey, and S. Tomsovic, Ann. Phys. **181**, 235 (1988).

[91] N. Dupuis and G. Montambaux, Phys. Rev. B **43**, 14390 (1991).

[92] P. Shukla, J. Phys. Condens. Matter **17**, 1653 (2005).

[93] K. Frahm and J.-L. Pichard, J. Phys. I (France) **5**, 847 (1995).

[94] S. Tomsovic, A. Lakshminarayan, S. C. L. Srivastava, and A. Bäcker, Phys. Rev. E **98**, 032209 (2018).

[95] V. Oganesyan and D. A. Huse, Phys. Rev. B **75**, 155111 (2007).

[96] Y. Y. Atas, E. Bogomolny, O. Giraud, and G. Roux, Phys. Rev. Lett. **110**, 084101 (2013).

[97] Y. Y. Atas, E. Bogomolny, O. Giraud, P. Vivo, and E. Vivo, J. Phys. A: Math. Theor. **46**, 355204 (2013).

[98] D. J. Luitz, N. Laflorencie, and F. Alet, Phys. Rev. B **91**, 081103(R) (2015).

[99] A. Pal and D. A. Huse, Phys. Rev. B **82**, 174411 (2010).

[100] E. Cuevas, M. Feigel'man, L. Ioffe, and M. Mezard, Nat. Commun. **3**, 1128 (2012).

[101] S. Kitamura, T. Oka, and H. Aoki, Phys. Rev. B **96**, 014406 (2017).

[102] A. Pandey, Ann. Phys. **119**, 170 (1979).

[103] M. Schiulaz, E. J. Torres-Herrera, F. Pérez-Bernal, and L. F. Santos, Phys. Rev. B **101**, 174312 (2020).

[104] E. J. Torres-Herrera, G. De Tomasi, M. Schiulaz, F. Pérez-Bernal, and L. F. Santos, Phys. Rev. B **102**, 094310 (2020).

[105] G. Lenz and F. Haake, Phys. Rev. Lett. **65**, 2325 (1990).

[106] S. Schierenberg, F. Bruckmann, and T. Wettig, Phys. Rev. E **85**, 061130 (2012).

[107] T. A. Brody, Lett. Nuovo Cimento **7**, 482 (1973).

[108] M. V. Berry and M. Robnik, J. Phys. A: Math. Gen. **17**, 2413 (1984).

[109] F. Schweiner, J. Laturner, J. Main, and G. Wunner, Phys. Rev. E **96**, 052217 (2017).

[110] F. M. Izrailev, J. Phys. A Math. Gen. **22**, 865 (1989).

[111] H. Hasegawa, H. J. Mikeska, and H. Frahm, Phys. Rev. A **38**, 395 (1988).

[112] G. Casati, F. Izrailev, and L. Molinari, J. Phys. A: Math. Gen. **24**, 4755 (1991).

[113] A. Y. Abul-Magd, J. Phys. A: Math. Gen. **29**, 1 (1996).

[114] A. L. Corps and A. Relaño, Phys. Rev. E **101**, 022222 (2020).

[115] S. Kullback and R. A. Leibler, Ann. Math. Statist. **22**, 79 (1951).

[116] S. Kullback, J. Appl. Phys. **24**, 106 (1953).

[117] S. Kullback, *Information Theory and Statistics* (Dover, New York, 1968).

[118] A. Gubin and L. F. Santos, Am. J. Phys. **80**, 246 (2012).

[119] See Supplemental Material at http://link.aps.org/supplemental/10.1103/PhysRevB.105.014205 for a detailed variation of $\langle r \rangle$ and $\langle \tilde{r} \rangle$ with h and J_t.